

# Efficient Diffusion Training through Parallelization with Truncated Karhunen-Loève Expansion

Yumeng Ren \*

ymren3-c@my.cityu.edu.hk

Yaofang Liu \*

yaofanliu2-c@my.cityu.edu.hk

Aitor Artola \*

aitor.artola@cityu.edu.hk

Laurent Mertz \*

lmertz@cityu.edu.hk

Raymond H. Chan<sup>†</sup>

raymond.chan@ln.edu.hk

Jean-michel Morel \*

jeamorel@cityu.edu.hk

## Abstract

Diffusion denoising models have become a popular approach for image generation, but they often suffer from slow convergence during training. In this paper, we identify that this slow convergence is partly due to the complexity of the Brownian motion driving the forward-time process. To address this, we represent the Brownian motion using the Karhunen-Loève expansion, truncating it to a limited number of eigenfunctions. We propose a novel ordinary differential equation with augmented random initials, termed *KL diffusion*, as a new forward-time process for training and sampling. By developing an appropriate denoising loss function, we facilitate the integration of our *KL-diffusion* into existing denoising-based models. Using the widely adopted *DDIM* framework as our baseline ensures a fair comparison, as our modifications focus solely on the forward process and loss function, leaving the network architecture and sampling methods unchanged. Our method significantly outperforms baseline diffusion models, achieving convergence speeds that are twice faster to reach the best FID score of the baseline and ultimately yielding much lower FID scores. Notably, our approach allows for highly parallelized computation, requires no additional learnable parameters, and can be flexibly integrated into existing diffusion methods. The code will be made publicly available.

## 1. Introduction

Recently, denoising diffusion models [8, 13, 24, 28] have emerged as crucial tools in synthetic data generation, with wide-ranging applications including text-to-image synthesis [21, 22, 29, 31] and conditional image generation [3, 17, 20, 30]; see [4] for a comprehensive survey. The framework

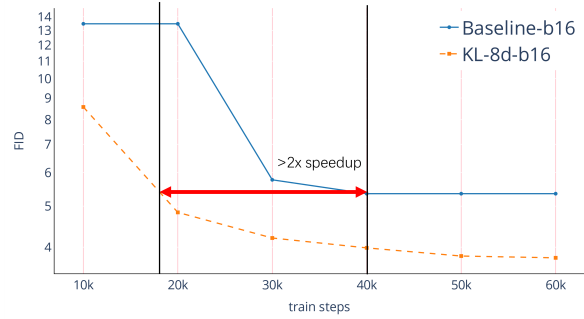


Figure 1. With the simplified and parallelized forward-time process, the same network trained with our KL loss (19) converges at least 2 times faster to a better FID score than that trained with existing score matching loss (7). The suffix **-8d** means the Karhunen-Lo  ve expansion is truncated to first 8 significant eigenfunctions and **-b16** means batch size is 16. See Figure 2(a) and Table 1 for details.

of stochastic differential equations [28] effectively captures the dynamics of both forward-time and reverse-time processes, facilitating the integration of various mathematical techniques to develop accelerated sampling algorithms [2, 15, 16, 24] and inverse problem solvers [10, 27, 32, 33]. However, a significant limitation of these models is their slow convergence during training, particularly evident in the forward-time process, which has not been extensively studied in the framework of stochastic processes in the literature [7, 13]. This paper aims to explore the intricacies of the forward-time process, ultimately leading to strategies for training acceleration.

In this paper, we investigate the challenge of slow convergence in training diffusion models, demonstrating that this issue partially stems from the complexity of the forward-time process used to generate the data for computing the training loss. Typically, achieving better train-

\*City University of Hong Kong

<sup>†</sup>Lingnan University of Hong Kong

ing results requires refined time discretization and a carefully weighted loss function [8, 28]. This complexity has been also highlighted from different perspectives [7], where conflicts in optimizing directions at different time steps are noted. We attribute this phenomenon to the independent increment nature of the Brownian motion  $W_t$  that drives the forward-time process, without a temporal derivatives in common sense (see "Ito calculus" in [18, 19]). Consequently, the temporal states in the forward process would not have path-wise derivatives in a normal sense. It leads to large fluctuations in optimizing the loss function, because the score function is fully defined in the forward-time process itself. Recently, the diffusion ordinary differential equations (diffusion ODEs) [13, 25, 28] provide competitive alternatives that keep the marginal distribution but modify the time dependencies. This observation inspires us to explore the structure of the Brownian motion that drives the forward-time process and discover efficient training schemes by limiting the temporal randomness.

To address this issue, we introduce the Karhunen-Loève (KL) expansion to explore the structure of the forward-time process. KL is a classical mathematical tool that represents a centered stochastic process  $X_t$  (i.e.,  $E[X_t] = 0$ ) as a linear combination of orthogonal time functions  $\phi_m(t)$ , where the coefficients  $Z_m$  are uncorrelated random variables, as expressed in the equation

$$X_t = \sum_{m=1}^{\infty} \phi_m(t) Z_m. \quad (1)$$

The orthogonal basis functions in this representation are derived from the covariance function of the process. In essence, the Karhunen-Loève transform adapts to the specific characteristics of the process to produce the most effective basis for its expansion. In our case, the targeted forward-time process is driven by Brownian motion over the time interval  $[0, 1]$ . Hence, the random variables  $Z_m$  are Gaussian and stochastically independent.

By reformulating the Brownian motion that is driving the forward-time process with a truncated expansion, we obtain a new family of ordinary differential equations (ODE) with augmented random initials, namely KL-diffusion model. In this framework, the time dependencies are expressed solely through determined time functions, while the independent random coefficients are shared along the path. Compared to the standard forward-time process, these ODEs maintain a similar marginal distribution and are driven by a Gaussian process, but with "limited directions," as they are truncated to the leading eigenfunctions and random coefficients. As a result, the KL-diffusion model shows a better path-wise smoothness and linearity in theory (Section 3.3), alleviating the conflicts during optimization across time steps. This is supported by significant acceleration observed in our experiments (Figure 2), measured by the number of optimiza-

tion steps required to achieve a descent generating quality level.

Specifically, our goal is to derive a trainable generative model based on the proposed KL-diffusion. The application and advantages of the Karhunen-Loève expansion differ from those in the traditional scenario of stochastic theory in several key aspects: (1) **Early Truncation**: The magnitude of  $|\phi_m|$  diminishes as  $m$  increases. To balance computational cost and performance, we prefer truncating the expansion to a few terms. (2) **Parallel Computation**: To design an efficient training and sampling algorithm, we emphasize that the predictions of each random coefficient are performed in parallel while the orthogonal basis functions remain fixed and shared through both training and sampling phases. (3) **Adaptable basis**: Although the random coefficients  $Z_m$  in the expansion serve as random initials, we allow the predicting network to incorporate time embeddings that jointly learn the time dependencies, enabling refinement of the predictions during the sampling loop. Detailed explanations can be found in Section 4.

Our proposed KL-diffusion simplifies vanilla diffusion models and naturally leads to a different training and sampling scheme in theory, however, with proper re-parametrization, it can be seamlessly applied to existing methods, such as DDPM and other denoising-based diffusion models. The sampler, network design and optimizer settings can be reused without introducing additional learnable parameters.

To conduct robust comparisons within the rapidly evolving field, we primarily focus on the application of our KL-diffusion to modify an existing denoising diffusion model (referred to as the baseline). We demonstrate improvements under identical settings for both training (including network structure and optimizer settings) and sampling (such as samplers and FID computation). Specifically, we utilize the noise scheduler functions and network architecture from the score-based model [28] and the sampler from DDIM [24] across several datasets of varying resolutions. Notably, our best FID scores are competitive with those of state-of-the-art methods.

Our contributions are summarized as follows:

- We identify the complexity of the forward-time process as a factor contributing to slow convergence in diffusion training and explore its structure using the Karhunen-Loève expansion, enabling further theoretical analysis.
- To the best of our knowledge, our KL-diffusion is the first approach to successfully incorporate the orthogonal expansion of a stochastic process into diffusion generative models, resulting in significant experimental improvements in training.

- Our proposed KL-diffusion can be seamlessly integrated into existing denoising-based diffusion models. Training the same network with KL diffusion achieves a better FID score in  $0.5\times$  optimization steps.

## 2. Related Works

### 2.1. diffusion models

Diffusion generative models have become mainstream methods for data synthesis, particularly in image and video generation. This broad family of techniques has expanded significantly since the foundational works [8, 26, 28], which have inspired numerous advancements aimed at improving sampling speed [24], denoising networks [4], noise schedules [9], degeneration procedure [1, 5] and other aspects. However, the fundamental forward- and backward-time processes have largely remained unchanged.

An important alternative to these traditional approaches is the ODE process [13, 24, 25, 28], which maintains the same marginal distribution as its stochastic differential equation (SDE) counterpart. Our method can be viewed as a family of ODEs with random initial conditions, contributing to the ongoing exploration of efficiency in diffusion generative models.

### 2.2. Karhunen-Loève expansion

In the theory of stochastic processes, the Karhunen-Loève (KL) expansion states that a stochastic process can be expressed as an infinite linear combination of orthogonal functions. This representation is analogous to the Fourier series representation of a function defined on a bounded interval and is a standard topic covered in textbooks [18, 19] on stochastic processes.

The Karhunen-Loève expansion is also applicable for generating random fields, which consist of a collection of random variables parameterized by a spatial variable  $x$  rather than a temporal one [6]. Additionally, it plays a significant role in developing numerical algorithms for partial differential equations with random coefficients [23].

In this paper, we concentrate on the expansion of Brownian motion, employing a truncation of the series to approximate Brownian motion effectively.

## 3. Method

In this section, we summarize the background of the standard diffusion generative model and the background of Karhunen-Loève expansion under unified notation and definitions. Then, we derive the core random differential equation for our KL-diffusion model.

### 3.1. Preliminaries of Denoising Diffusion Models

Diffusion models are composed of two processes described by a forward-time process and a reversed-time process,

formulated in stochastic differential equations (SDEs). In the following, we adopt the notation and equations from [28] and reformulate them for further use.

The forward-time process, for  $t \in [0, 1]$ , is given by

$$dX_t = f(t)X_t dt + g(t)dW_t, \quad (2)$$

$$X_0 \sim p_{\text{data}} = \frac{1}{N} \sum_{j=1}^{N_{\text{data}}} \delta_{x_j}(\cdot)$$

where the data set can be written as  $\{x_j\}_{j=1}^{N_{\text{data}}}$ . This stochastic process initiates from a data distribution  $p_{\text{data}}$  and is driven by a Brownian motion  $W_t$ , where  $f(t)$  and  $g(t)$  are scalar functions that control the noise level schedule. An explicit solution to the forward-time process is

$$X_t = \exp\left(\int_0^t f(s)ds\right) X_0 + \int_0^t \exp\left(\int_s^t f(r)dr\right) g(s)dW_s. \quad (3)$$

In this paper, we adopt the following parameterization  $f(t) = -\frac{1}{2}\beta(t)$ ,  $g(t) = \sqrt{\beta(t)}$ , consistent with the variance-preserving SDE (VE-SDE) [28]. In the experiments of this paper, we use  $\beta(t) = 0.1 + 19.9t$  as in the standard implementation of VE-SDE. Consequently, equation (3) becomes

$$X_t = \mu(t)X_0 + \int_0^t \frac{\mu(t)}{\mu(s)} \sqrt{\beta(s)}dW_s, \quad (4)$$

where  $\mu(t) = \exp\left(-\int_0^t \frac{1}{2}\beta(s)ds\right)$ . Other choices of  $\beta(t)$  [9, 28] would not change any of the theoretical derivations of this paper.

Sampling with score function is accomplished by solving the reversed-time process. Let  $p_{\sigma(t)}(\tilde{x}|x) := p_{\sigma(t)}(X_t = \tilde{x}|X_0 = x) = \mathcal{N}(\mu(t)x, \sigma(t)^2 I)$  and  $p_{\sigma(t)}(X_t = \tilde{x}) = \int p_{\sigma(t)}(\tilde{x}|x)p_{\text{data}}(x)dx$ . We show the reversed-time process, for  $t \in [0, 1]$ , as below

$$dX_t = -\left[\frac{1}{2}X_t + \nabla_{\tilde{x}} \log p_{\sigma(t)}(X_t)\right]\beta(t)dt + \sqrt{\beta(t)}dW_t, \quad (5)$$

$$X_1 \sim \mathcal{N}(0, I).$$

With proper time discretization and approximation, many different samplers, like DDIM [24], can be applied to solve the reversed-time process.

The score-matching loss function for training is

$$\mathbb{E}_{x \sim p_{\text{data}}} \mathbb{E}_{\tilde{x} \sim p_{\sigma}(\tilde{x}|x)} \left\| s_{\theta}(\tilde{x}, \sigma(t)) + \frac{\tilde{x} - \mu(t)x}{\sigma(t)^2} \right\|_2^2, \quad (6)$$

where  $s_{\theta}$  is the model to fit the score function. In practice [8, 28], it is further re-parameterized as a denoising loss function as follow

$$\ell(\theta, t) = \mathbb{E}_{x \sim p_{\text{data}}} \mathbb{E}_{x_t = \mu(t)x + \sigma(t)Z_t} \mathbb{E}_{Z_t \sim \mathcal{N}(0, 1)} \|Z_t - Z_{\theta}(x_t, \sigma(t))\|_2^2, \quad (7)$$

where  $Z_{\theta}$  is the denoising network.

### 3.2. Karhunen-Loève Expansion

In order to explore and replace the driving process in the standard forward-time process, we focus on one of the special results of the Karhunen-Loève expansion (1), which decomposes a Brownian motion  $W_t$  on the time interval  $[0, 1]$ :

$$W_t = \sum_{m=1}^{\infty} Z_m \phi_m(t) \text{ for } 0 \leq t \leq 1, \quad (8)$$

where  $Z_1, Z_2, \dots, Z_m, \dots$  are independent standard Gaussian random variables and the functions  $\phi_1, \phi_2, \dots, \phi_m, \dots$  are sinusoidal functions defined as  $\phi_m(t) = \frac{2\sqrt{2}}{(2m-1)\pi} \sin\left(\frac{(2m-1)\pi t}{2}\right)$ . We then truncate this expansion to its first  $M$  terms by setting

$$W_t^M = \sum_{m=1}^M \phi_m(t) Z_m. \quad (9)$$

This truncation retains the first  $M$  eigenfunctions. It simplifies the noising process by using a limited number of basis terms, yet producing an optimal approximation of the Brownian motion. The optimality of this approximation by the KL expansion and its truncated formulation is well-covered in the literature [18, 19].

### 3.3. KL diffusion

To associate a forward-time process with our new driving process, we first compute the derivatives of the truncated expansion (8),

$$\dot{W}_t^M = \sum_{m=1}^M \dot{\phi}_m(t) Z_m, \quad (10)$$

where  $\dot{\phi}_m(t) = \frac{d\phi_m(t)}{dt}$ . Then, we introduce our **KL diffusion** as an ODE, with augmented random initials,  $\mathbf{Z}^M = (Z_1, Z_2, \dots, Z_M)$ , along with the data distribution  $p_{\text{data}}$  as below

$$\begin{aligned} \dot{X}_t^M &= -\frac{1}{2}\beta(t)X_t^M + \sqrt{\beta(t)}\dot{W}_t^M, \\ X_0^M &\sim p_{\text{data}}, \quad \mathbf{Z}^M \stackrel{\text{iid}}{\sim} \mathcal{N}(0, I)^M. \end{aligned} \quad (11)$$

It has a unique explicit solution

$$X_t^M = \mu(t)X_0 + \sum_{m=1}^M h_m(t)Z_m, \quad (12)$$

where  $h_m(t) = \int_0^t \sqrt{\beta(s)} \frac{\mu(t)}{\mu(s)} \dot{\phi}_m(s) ds$ . This formulation has the useful property that

$$V[X_t^M] = \sum_{m=1}^M h_m(t)^2 \rightarrow V[X_t] = \sigma(t)^2, \quad (13)$$

where  $\sigma(t)$ ,  $\mu(t)$  and  $\beta(t)$  are defined in Section 3.2.

We anticipate that this simplification not only preserves the essential characteristics of the original process but also enhances the training efficiency of the networks. This allows denoising networks to focus on the most significant modes of variation, thus improving the quality of generation tasks with a properly designed training scheme.

### 4. Training algorithms based on KL-diffusion

Here we define a new loss function based on the KL-diffusion (11), matching the gradient flow of the driving process with a deep network  $v_{\theta}$ ,

$$\mathbb{E}_{\substack{x \sim p_{\text{data}} \\ \mathbf{Z}^M \sim \mathcal{N}(0, I)^M}} \|\dot{X}_t^M - v_{\theta}(X_t^M, t)\|_2^2 \quad (14)$$

It is very different from the re-parametrization of the denoising loss in (7). However, the process can be reformulated and approximated based on (12) as follows:

$$X_t^M \approx \mu(t)X_0 + \frac{\sigma(t)}{\sqrt{t}} \sum_{m=1}^M \phi_m(t) Z_m, \quad (15)$$

in the sense of  $\mathbb{E}[X_t^M] = \mathbb{E}[\tilde{X}_t^M]$  and  $\mathbb{V}[X_t^M] \approx \mathbb{V}[\tilde{X}_t^M]$ , since we know that  $\sum_{m=1}^{\infty} \phi_m^2(t) = t$  and  $\lim_{m \rightarrow \infty} |\phi_m(t)| = 0$ . Let  $Z'_t := \sum_{m=1}^M \frac{\phi_m(t)}{\sqrt{t}} Z_m$  then we have

$$X_t^M \approx \tilde{X}_t^M := \mu(t)X_0 + \sigma(t)Z'_t \quad (16)$$

and it enables to re-parameterize a denoising loss function

$$\mathbb{E}_{x \sim p_{\text{data}}} \mathbb{E}_{\substack{\mathbf{Z}^M \sim \mathcal{N}(0, I)^M \\ \tilde{x} = \mu(t)x + \sigma(t)Z'_t}} \left\| Z'_t - \sum_{m=1}^M \frac{\phi_m(t)}{\sqrt{t}} Z_{\theta}(\tilde{x}, m) \right\|_2^2. \quad (17)$$

In practice, it can potentially alleviate the burden of training to allow the basis function to be adapted. So the loss function further re-parameterized as

$$\mathbb{E}_{x \sim p_{\text{data}}} \mathbb{E}_{\substack{\mathbf{Z}^M \sim \mathcal{N}(0, I)^M \\ \tilde{x} = \mu(t)x + \sigma(t)Z'_t}} \left\| \sum_{m=1}^M \left( \frac{\phi_m(t)}{\sqrt{t}} Z_m - \hat{Z}(\tilde{x}, m, t, \theta) \right) \right\|_2^2 \quad (18)$$

where  $\hat{Z}(x, m, t, \theta) := \frac{\phi_m(t)}{\sqrt{t}} \tilde{Z}_{\theta}(x, m, t)$  to jointly learn the product of time basis and random coefficient. Compared to the derivative matching loss (14), the denoising loss (18) has the advantage that a trained network  $\tilde{Z}_{\theta^*}$  can be seamlessly used in any existing denoising-based sampling algorithms, since (17) is analogous to the existing denoising loss function (7). Furthermore, under a specific time discretization

$t_k = k/N, (0 \leq k \leq N)$  and  $N = 1000$ , the loss function (18) can be implemented as

$$\ell_{\text{KL}}(\theta, t_k) = \mathbb{E}_{x \sim p_{\text{data}}} \mathbb{E}_{\mathbf{Z}^M \sim \mathcal{N}(0, I)^M} \mathbb{E}_{\tilde{x} = \mu(t_k)x + \sigma(t_k)Z'_{t_k}} \left\| \sum_{m=1}^M \phi_m(t_k) (Z_m - \tilde{Z}_\theta(\tilde{x}, N(m-1) + k)) \right\|_2^2, \quad (19)$$

where  $\tilde{Z}_\theta(\tilde{x}, \cdot)$  can be a denoising network with a time-embedding input as in [28]. We denote (19) as **KL loss** in the rest of the paper.

Such a re-parameterized loss function (19) enables us to conduct strict comparison to show the power of KL diffusion. The experiments Section 6.3 focuses on training and comparing the denoising diffusion baseline with and without our KL-diffusion, i.e., with the proposed loss function (19) or with the original loss function (7). The proposed KL-diffusion training method is summarized in Algorithm 1.

#### NOTE 1

In (17), (18) and (19), the noise to be estimated are the same, that is,  $Z'_t$ . But we use different ways to embed  $(m, t)$  or  $(m, t_k)$  into a trainable network,  $Z_\theta(\tilde{x}, m)$  for (17),  $\tilde{Z}_\theta(\tilde{x}, m, t)$  for (18) and  $\tilde{Z}_\theta(\tilde{x}, N(m-1) + k)$  for (19). These three loss functions can be regarded as different solvers for our KL diffusion (11).

#### NOTE 2

The computation of the gradient for the loss function (19) is expensive due to the  $M$  times evaluations of the network  $\tilde{Z}_\theta$  required per optimizing step. This computational cost can be mitigated by predicting  $\tilde{Z}_\theta$  in parallel. Consequently, in implementation, the effective batch size for the input of  $\tilde{Z}_\theta$  is equal to the product of image batch size and the number of basis terms  $M$ .

#### NOTE 3

Based on (19), we can conduct a trade-off between time and space (i.e., VRAM) by partially collecting the gradients of the predictions of basis terms during the optimization step. For  $M' < M$ , we define the **KL partial loss** as

$$\ell(\theta, t_k; \{m_j\}_{j=1}^{M'}) = \mathbb{E}_{x \sim p_{\text{data}}} \mathbb{E}_{\mathbf{Z}^M \sim \mathcal{N}(0, I)^M} \mathbb{E}_{\tilde{x} = \mu(t_k)x + \sigma(t_k)Z'_{t_k}} \frac{1}{t_k} \sum_{j=1}^{M'} \left\| Z_{m_j} - \tilde{Z}_\theta(\tilde{x}, N(m_j-1) + k) \right\|_2^2, \quad (20)$$

where  $\{m_j\}$  is a randomly selected subsequence from  $\{1, 2, \dots, M\}$ . The motivation is that when  $M' = M$  and  $\{m_j\} = \{1, 2, \dots, M\}$ , minimizing (20) is equal to minimize an upper bound of (19), which is proved as below

$$\begin{aligned} \left\| \sum_{m=1}^M \phi_m(t) (Z_m - \tilde{Z}_\theta) \right\|_2^2 &\leq \left\| \sum_{m=1}^M (Z_m - \tilde{Z}_\theta) \right\|_2^2 \\ &\leq \sum_{m=1}^M \|Z_m - \tilde{Z}_\theta\|_2^2 \end{aligned}$$

since  $|\phi_m(t)| \geq 1$ .

The KL partial loss (20) could provide a descent network training and gradually catch up the case using full KL loss as  $M'$  increasing; These analysis are supported by our experiments in Section 6.4.

---

#### Algorithm 1 Training with KL loss

---

- 1: Randomly select  $x \sim p_{\text{data}}$  from the image dataset,
- 2: Sample  $Z_1, Z_2, \dots, Z_M \sim \mathcal{N}(0, I)$  iid.
- 3: Randomly select  $t_k \in \{t_1, t_2, \dots, t_N\}$ ,
- 4: Compute

$$Z'_{t_k} = \sum_{m=1}^M \phi_m(t_k) Z_m \quad (21)$$

$$\tilde{x}_{t_k} = \mu(t_k)x_0 + \sigma(t_k) \sum_{m=1}^M \phi_m(t_k) \tilde{Z}_\theta(x_{t_k}, N(m-1) + k) \quad (22)$$

- 5: Apply the gradient descent step (Adam) towards the loss function (19).
- 

## 5. Sampling algorithm based on KL diffusion

If a network  $Z_\theta(X_t, m, i)$  is trained with loss function (19), it can be sampled by any samplers for standard denoising diffusion models. In this paper, we take the DDIM sampler [24], because it is a widely used sampler that shares its structure with many others, and because it has a good trade-off between quality and sampling speed.

DDIM [24] improves the standard diffusion by considering only a subset  $\{t_{k_i}\}_{i \in \cdot}$  of the set of discretized time steps  $\{t_k = k/N\}_{k \in [0; N]}$  with  $N = 1000$ . The sampling step of DDIM from  $t_{k_i}$  to  $t_{k_{i-1}}$  is defined as:

$$\begin{aligned} X_{k_{i-1}} &= \sqrt{\bar{\alpha}_{k_{i-1}}} \left( \frac{X_{k_i} - \sqrt{1 - \bar{\alpha}_{k_i}} \cdot \hat{\epsilon}}{\sqrt{\bar{\alpha}_{k_i}}} \right) \\ &\quad + \sqrt{1 - \bar{\alpha}_{k_{i-1}} - (\eta \tilde{\sigma}_{k_i})^2} \cdot \hat{\epsilon} + \eta \tilde{\sigma}_{k_i} z, \quad z \sim \mathcal{N}(0, I) \end{aligned} \quad (23)$$

where  $X_{k_i}$  is alias to  $X_{t_{k_i}}$  and  $\hat{\epsilon}$  is the noise to be estimated. The noise schedule arguments are defined as follows:

$$\begin{aligned}\bar{\alpha}_k &= \mu(t_k)^2, \\ \alpha_k &= \bar{\alpha}_k / \bar{\alpha}_{k-1}, \\ \tilde{\sigma}_{k_i} &= \sqrt{\frac{1 - \alpha_{k_{i-1}}}{1 - \alpha_{k_i}}} \sqrt{1 - \frac{\alpha_{k_i}}{\alpha_{k_{i-1}}}}\end{aligned}$$

which are the same as in [24]. In our experiments, we choose DDIM( $S = 20, \eta = 1$ ) to generate images and compute FID scores.

In the baseline the noise  $\hat{\epsilon}$  is directly predicted by a network trained with the loss (7). In our alternative, the network  $Z_{\theta^*}(\tilde{x}, Nm + k)$  trained with the loss (19), estimate the noise  $\hat{\epsilon}$  as an aggregation of its outputs :

$$\hat{\epsilon} = \frac{1}{\sqrt{t_{k_i}}} \sum_{m=1}^M \phi_m(t_{k_i}) \tilde{Z}_{\theta}(X_{k_i}, N(m-1) + i). \quad (24)$$

In this manner, any existing sampling algorithm that based on denoising networks can works with the KL diffusion. It also enable use to conduct strict comparison in which the only modification is that denoising sub-procedure in training loss and sampling step is replaced by a version with KL diffusion.

## 6. Experiment

In this section, we provide an overview of our experiments. We begin by presenting the main results related to training speedup, followed by a comprehensive ablation study and discussions that align with the theoretical properties discussed in previous sections.

### 6.1. Datasets

**MNIST-32** The MNIST dataset [12] comprises 70000 grayscale images representing 10 classes, from digit 0 to digit 9. All images are rescaled to  $32 \times 32 \times 1$ . We select this dataset for extensive training and FID computations to explore the properties of KL-diffusion as outlined in our theoretical analysis.

**CIFAR10-32** The CIFAR10 dataset [11] contains 60000 images of  $32 \times 32 \times 3$  in 10 classes, with 6000 images per class.

**CelebAHQ-64 and CelebAHQ-128** We conduct experiments on the CelebAHQ dataset [14], which consist of 30,000 images. They are rescaled into two resolution levels,  $64 \times 64 \times 3$  and  $128 \times 128 \times 3$ .

We take the same augmentation pipeline on all datasets, including random flip and normalization. Mention that for all resolution image generation, we directly train the diffusion model on the pixel-level.

### 6.2. Training Details

We borrow the denoising network design from [8]. We use an fixed U-Net architecture for all experiments. A network trained with KL-diffusion loss (19) using  $M$  terms is denoted as **KL-Md**. A network trained with KL partial loss (20) using  $M$  terms in truncation and  $M'$  terms in loss function is denoted as **KL-MdM'**. A network trained with the standard loss (7) is referred to as **Baseline**. An optional suffix **-bB** indicates that a model is trained with a batch size of  $B$ . If not specific, the time discretization for KL models are  $N = 20$  since it will improve the performance compared to  $N = 1000$ ; and the time discretization for baseline models is  $N = 1000$  since the  $N = 20$  will dramatically decrease the performance of baseline.

Experiments are conducted in a mixed hardware environment. Training sessions utilize a single RTX 3090 (24 GB) card for experiments on MNIST-32, CIFAR10-32 and CelebAHQ-64 and a single H800 (80GB) card for CelebAHQ-128. Gradient accumulation and Automatic Mixed Precision (AMP, fp16) are enabled. We use AdamW optimizer, Exponential Moving Average (EMA) and other default training settings from a popular implementation of diffusion training (<https://github.com/lucidrains/denoising-diffusion-pytorch>). We select the DDIM sampler ( $\eta = 1, S = 20$ ) in (23) to sample images and FID computation (50k generated images).

Our experimental design involves a large number of trainings and FID computations to have a comprehensive comparison between the baseline and our model in configurations of different batch size and number of basis  $M$  in KL diffusion. Note that, due to limitation of time and devices, each experiment has far smaller batch size and far smaller total training steps compared to [7, 8, 24, 28] in which usually have batch size greater than 64 and total steps greater than 500k.

Mention that the choices above are to achieve rapid training and sampling. It is crucial given the extensive number of trainings and FID computations required for our comprehensive comparisons, effectively exploring the properties of our KL-diffusion across various settings. Although this configuration may yield lower-quality samples than the state-of-the-art records, it can be easily extended to slower, higher-quality sampling methods, like the DDIM( $S = 100, \eta = 0$ ) sampler as shown in [24].

### 6.3. Comparison between the networks trained with and without KL diffusion

To demonstrate the effectiveness of our KL-diffusion approach, we conduct experiments comparing networks trained with and without our KL loss functions (19). The comparison between the baseline and KL models is conducted rigorously, using exactly the same network architecture. The only difference is the application of our KL

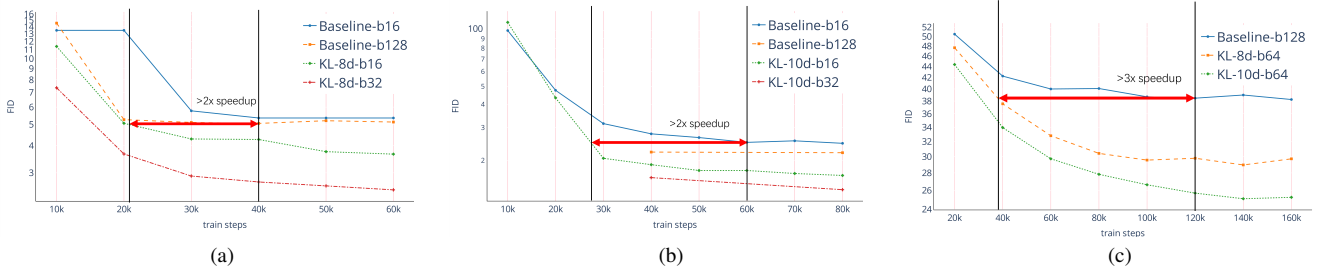


Figure 2. Comparisons between the baseline with KL diffusion on datasets, (a) for MNIST-32, (b) for CelebAHQ-64 and (c) for CIFAR10-32. Our method (KL-8d-16b) converges to better FID scores at least 2 times faster than baseline (Baseline-16b) with the same batch size 16 and have even better FID than baseline of batch size 16 or 128 (Baseline-16b, Baseline-128b). See Section 6.3 for details.



Figure 3. Samples generated on specific optimizing steps. The first row is from **Baseline-b16** at 8k, 16k, 24k and 32k steps, from (a) to (d). The second row is from **KL-8d-32b** at the same steps, from (e) to (h). Our **KL-8d-b32** have larger quality gain every 8k steps and quickly learn to generated better samples comparing to the **Baseline-b16**.

denoising loss, while all other settings remain consistent.

Figure 2 presents comparisons for networks trained on the MNIST-32, Celeb-64 and CIFAR10-32 datasets. First, in sub-figures (a) and (b), to ensure a fair evaluation of our **KL-8d**, we consider two trained networks: **Baseline-b16** and **Baseline-b128**. The former matches a case to consume the same number of different images per optimization step, while the latter maintains the same actual batch size due to parallelized computation, as discussed in Section 4 (NOTE 2). In both cases, our method achieves superior FID scores with significantly fewer optimization steps, above 2 times

speed-up. In addition, when trained with a larger batch size, our **KL-8d-b32** model exhibits even better performance. Second, in sub-figure (c), we show results of **KL-8d** and **KL-10d** with a larger batch size as 64, the speed-up effect is dramatically improved to more than 3 times comparing to **Baseline-128** on CIFAR10-32 dataset. A visual demonstration the speed-up effect is given in Figure 3, comparing **KL-8d-32b** and **Baseline-16b** trained on Celeb64 dataset. More results on higher resolution (CelebAHQ-128) are shown in Appendix D.

The raw data supporting the findings of Figure 2 are

Best FID(↓)	DDIM	Baseline-b16	Baseline-b128	KL-8d-b16	KL-8d-b32
MNIST-32	-	5.35	5.05	3.60	2.44
Best FID	DDIM	Baseline-b16	Baseline-b128	KL-8d-b16	KL-8d-b32
CelebAHQ-64	26.03	24.66	22.00	16.61	14.2
Best FID (↓)	DDIM	Baseline-b128		KL-8d-b64	KL-10d-b64
CIFAR10-32	18.36	38.21		28.97	25.10

Table 1. Comparison of the best FID achieved in training for the baselines and our model. The 2nd column is the FID reported in DDIM ( $S = 20$ ,  $\eta = 1$ ) [24]. The 3rd and 4th columns are the same network as DDIM but trained by us standard loss function. The 5th and 6th column is the same network trained by KL loss. The improvements of KL models are significant in all cases.

presented in Table 1. For the MNIST dataset, **KL-8d-b16** rapidly surpasses the best FID score of 5.35 achieved by **Baseline-b16** using only half the number of optimization steps, eventually reaching a much lower FID score of 3.65. Similar significant improvements are observed on CelebAHQ-64 and CIFAR10-32. We also provide reference FID scores from DDIM for both the Baseline and KL models we trained. Notice that, compared with scores from DDIM, our reproduced baselines perform better on CelebAHQ-64 but worse on CIFAR10-32; however, the application of the KL training loss consistently leads to significant and robust improvements in all cases. Mention that, our methods can seamlessly integrate with any state-of-the-art techniques derived from denoising-based diffusion models, as stated in Section 4 and 5.

#### 6.4. Trade-off Between Training Cost and Performance Using Partial KL Loss Function

Our KL loss (19) provide a far better optimizing direction compared to the standard one (7), however, the gradient for certain terms, as indicated in (20), rather than relying on the full truncated expansion. While this approach may slightly diminish the speed-up effect, it still converges to a comparable FID level as networks trained with the complete KL loss (19).

Figure 4 illustrates that as  $M'$  increases, the FID score decreases, gradually approaching the curve for **KL-10d**, which was trained with the full KL loss. This simple yet effective trade-off scheme makes our KL method flexible, enabling deployment on resource-constrained devices while achieving high efficiency on larger computational nodes. The space and time cost estimated on baselines and our models is shown in Table 2 illustrating the effectiveness of KL partial loss.

The number of terms,  $M$ , is a hyperparameter also influence the cost and performance of KL models. We discuss the impact of differencet  $M$  in Appendix A.

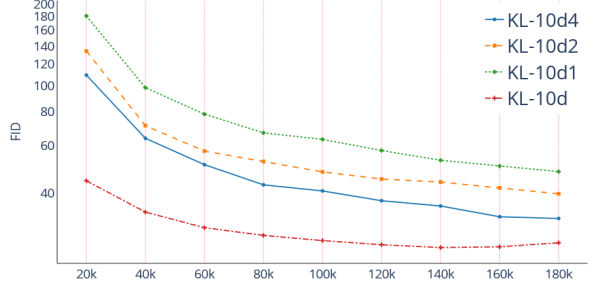


Figure 4. Comparison of networks with the same architecture trained on the CIFAR10-32 using the KL loss and KL partial loss with  $M' = 4, 2$ , and 1 whose best FIDs in 180k steps are 25.10, 32.16, 39.69 and 47.97, separately.

	Baseline-b16	KL-10d1-b16	KL-10d4-b16	KL-8d	KL-10d
VRAM(MB)	3241	3256	8006	15225	18848
Time(10k steps)	4h37m	4h55m	10h37m	13h59m	16h39m

Table 2. The space (VRAM) and time (scaled to 10k steps) cost for training baseline models and our KL models.

#### 6.5. Reduce Time Cost by Alternating Network Architecture

The cost in time for each timestep is high for the implementation above (denoted **KL**<sup>1st</sup>), but it may not be a fundamental limitation of KL diffusion. To address this issue, we introduce a second implementation **KL**<sup>2nd</sup>. This version also retains the same network architecture  $\tilde{Z}_\theta$  as the classical diffusion, but introduce a few more learnable parameters by expanding the last convolution layer to have  $M$  times larger output channels. That means, the new network  $\tilde{Z}_\theta^{2nd}(x, t)$  provides  $M$  predictions of all coefficients in one pass. Thus, the corresponding loss function can be defined as

$$\ell_{\text{KL}^{2nd}}(\theta, t_k) = \mathbb{E}_{x \sim p_{\text{data}}} \mathbb{E}_{\mathbf{Z}^M \sim \mathcal{N}(0, I)^M} \frac{1}{t_k} \left\| \phi(t_k) \cdot \left( Z - \tilde{Z}_\theta^{2nd}(\tilde{x}, k) \right) \right\|_2^2, \quad (25)$$

where  $\phi(t) = (\phi_1(t), \phi_2(t), \dots, \phi_M(t))$ ,  $Z = (Z_1, Z_2, \dots, Z_M)$  and the operation  $\cdot$  stands for inner product along the dim of channels.

Figure 5 shows that on the CIFAR10-32 with one RTX 3090 24G card, **KL**<sup>2nd</sup> has a slightly higher FID than **KL**<sup>1st</sup>, but it reduces the time cost to the baseline level. Therefore, computational inefficiency is not a fundamental flaw of the KL diffusion but a question of implementations.

For further clarification, the time reported in Table 2 also includes periodic evaluations such as FID computations, while the time in Figure 5 only refers to the optimization steps; also, the number of score function evaluations (NFE)

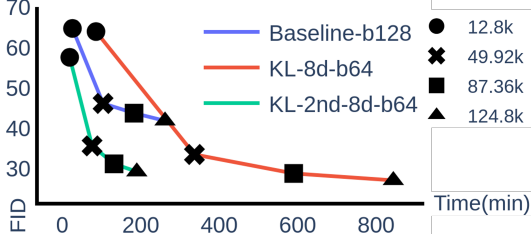


Figure 5. Compare the training costs of time and steps on the CIFAR10-32 dataset.

Steps	3.12k	12.48k	49.92k
KL-8d-b16(w/o)	-	89.23	53.03
KL-8d-b16(w)	49.96	37.76	36.85
KL <sup>2nd</sup> -8d-b16(w/o)	-	83.02	60.22
KL <sup>2nd</sup> -8d-b16(w)	38.72	38.27	37.83

Table 3. Compare the performance on the CIFAR10-32 dataset between the networks (w) initialized with pretrained classical diffusion (baseline-b128, trained with 124.8k steps, FID=40.37) and those trained from scratch (w/o).

is the same for  $\mathbf{KL}^{1st}$ ,  $\mathbf{KL}^{2nd}$  and the baseline. In  $\mathbf{KL}^{1st}$ , we achieve  $M$  predictions using a batch size  $M$  times larger with  $M$  duplications of input images, instead of looping  $M$  times.

## 6.6. Fine-tuning KL models based on a pretrained diffusion model

As shown in (17), the expansion  $\sum_{m=1}^M \frac{\phi_m(t)}{\sqrt{t}} Z_{\theta^*}$  replaces the noise predictor  $\epsilon_{\theta^*}$ . To enable fine-tuning, we directly load the weights  $\theta^*$  from  $\epsilon_{\theta^*}$  to  $Z_{\theta^*}$ , since they share architectures. And then, apply a correction as  $Z_{\theta^*}^{\dagger} = \sqrt{t} Z_{\theta^*} / \sum_{m=1}^M \phi_m(t)$ . In  $\mathbf{KL}^{1st}$ , we approximate  $\epsilon_{\theta^*} \approx \sum_{m=1}^M \frac{\phi_m(t)}{\sqrt{t}} Z_{\theta^*}^{\dagger}$  following the fact that  $Z_{\theta^*}(x, N(m-1) + k) = \epsilon_{\theta^*}(x, k)$  when  $m=1$  and  $t=t_k$ . The first term  $\phi_1(t)$  has a bigger impact than the higher-order terms, which rapidly diminish at a rate of  $O(\frac{1}{2m-1})$ , as shown in (8). For  $\mathbf{KL}^{2nd}$ , we initialize the additional weights in the last convolution by copying, so that  $\epsilon_{\theta^*}(x, k) = Z_{\theta^*}(x, N(m-1) + k)$  for  $m = 1, 2, \dots, M$ , and  $\epsilon_{\theta^*} = \sum_{m=1}^M \frac{\phi_m(t)}{\sqrt{t}} Z_{\theta^*}^{\dagger}$ . As shown in Table 3, the weights from a pretrained diffusion model provides a far better start.

## 7. Conclusion

In this paper, we investigate the driving process of the forward-time operation in denoising diffusion models and introduce KL diffusion, a novel diffusion process represented as a family of ordinary differential equations (ODEs) with augmented random initials. To our knowledge, this is the first work to incorporate the Karhunen-Loeve expansion into diffusion model design. We propose a flexible training

scheme called KL loss, which integrates seamlessly into existing denoising-based models.

Our comprehensive comparisons show that networks trained with KL loss significantly outperform the baseline (without KL loss) in only 0.5 to 0.33 times the optimization steps and converging to better FID scores. We also introduce KL partial loss to balance computational cost with quality gains.

Overall, based on our current experiments, the loss functions (19) and (20) based on KL diffusion provide far better optimizing directions albeit at a higher computational expense per step. Ultimately, they converge to points with superior FID scores compared to the existing score matching loss (7). This suggests that the forward process based on KL diffusion facilitates a more effective transition between data distribution and Gaussian distribution. There is significant value in exploring more efficient solvers for KL diffusion, as it demonstrates promising performance but requires optimization for greater efficiency.

Due to time constraints, this paper presents only one alternative approach to addressing KL diffusion (see NOTE 2, the partial KL loss). Future work may explore more computational efficient optimization strategies for KL diffusion, such as utilizing general orthogonal basis families of temporal sparsity, and applying these advancements to modern denoising architectures like Vision Transformers (ViT) to match state-of-the-art performance.

## References

- [1] Arpit Bansal, Eitan Borgnia, Hong-Min Chu, Jie Li, Hamid Kazemi, Furong Huang, Micah Goldblum, Jonas Geiping, and Tom Goldstein. Cold diffusion: Inverting arbitrary image transforms without noise. *Advances in Neural Information Processing Systems*, 36:41259–41282, 2023. 3
- [2] Fan Bao, Chongxuan Li, Jun Zhu, and Bo Zhang. Analytic-DPM: An Analytic Estimate of the Optimal Reverse Variance in Diffusion Probabilistic Models. In *International Conference on Learning Representations (ICLR)*. arXiv, May 2022. 1
- [3] Guillaume Couairon, Marlene Careil, Matthieu Cord, Stéphane Lathuiliere, and Jakob Verbeek. Zero-shot spatial layout conditioning for text-to-image diffusion models. In *Proceedings of the IEEE/CVF International Conference on Computer Vision*, pages 2174–2183, 2023. 1
- [4] Florinel-Alin Croitoru, Vlad Hondru, Radu Tudor Ionescu, and Mubarak Shah. Diffusion models in vision: A survey. *IEEE Transactions on Pattern Analysis and Machine Intelligence*, 45(9):10850–10869, 2023. 1, 3
- [5] Giannis Daras, Mauricio Delbracio, Hossein Talebi, Alex Dimakis, and Peyman Milanfar. Soft diffusion: Score matching with general corruptions. *Transactions on Machine Learning Research*. 3
- [6] Roger G Ghanem and Pol D Spanos. *Stochastic Finite Elements: A Spectral Approach*. Courier Corporation, 2003. 3

- [7] Tiankai Hang, Shuyang Gu, Chen Li, Jianmin Bao, Dong Chen, Han Hu, Xin Geng, and Baining Guo. Efficient Diffusion Training via Min-SNR Weighting Strategy. In *2023 IEEE/CVF International Conference on Computer Vision (ICCV)*, pages 7407–7417, Paris, France, Oct. 2023. IEEE. 1, 2, 6
- [8] Jonathan Ho, Ajay Jain, and Pieter Abbeel. Denoising Diffusion Probabilistic Models. *Advances in neural information processing systems*, 33:6840–6851, 2020. 1, 2, 3, 6
- [9] Tero Karras, Miika Aittala, Timo Aila, and Samuli Laine. Elucidating the Design Space of Diffusion-Based Generative Models, Oct. 2022. 3
- [10] Bahjat Kawar, Gregory Vaksman, and Michael Elad. SNIPS: Solving Noisy Inverse Problems Stochastically, Nov. 2021. 1
- [11] A Krizhevsky. Learning multiple layers of features from tiny images. *Master’s thesis, University of Tront*, 2009. 6
- [12] Yann LeCun, Léon Bottou, Yoshua Bengio, and Patrick Haffner. Gradient-based learning applied to document recognition. *Proceedings of the IEEE*, 86(11):2278–2324, 1998. 6
- [13] Xingchao Liu, Chengyue Gong, and Qiang Liu. Flow Straight and Fast: Learning to Generate and Transfer Data with Rectified Flow, Sept. 2022. 1, 2, 3
- [14] Ziwei Liu, Ping Luo, Xiaogang Wang, and Xiaoou Tang. Deep learning face attributes in the wild. In *Proceedings of the IEEE International Conference on Computer Vision*, pages 3730–3738, 2015. 6
- [15] Cheng Lu, Yuhao Zhou, Fan Bao, Jianfei Chen, Chongxuan Li, and Jun Zhu. Dpm-solver: A fast ode solver for diffusion probabilistic model sampling in around 10 steps. *Advances in Neural Information Processing Systems*, 35:5775–5787, 2022. 1
- [16] Simian Luo, Yiqin Tan, Longbo Huang, Jian Li, and Hang Zhao. Latent consistency models: Synthesizing high-resolution images with few-step inference. *arXiv preprint arXiv:2310.04378*, 2023. 1
- [17] Rishabh Parihar, VS Sachidanand, Sabariswaran Mani, Tejan Karmali, and R Venkatesh Babu. Precisecontrol: Enhancing text-to-image diffusion models with fine-grained attribute control. In *European Conference on Computer Vision*, pages 469–487. Springer, 2024. 1
- [18] Grigorios A. Pavliotis. *Stochastic Processes and Applications: Diffusion Processes, the Fokker-Planck and Langevin Equations*, volume 60 of *Texts in Applied Mathematics*. Springer New York, New York, NY, 2014. 2, 3, 4
- [19] Peter E. Kloeden and Eckhard Platen. *Numerical Solution of Stochastic Differential Equations*, volume 23 of *Stochastic Modelling and Applied Probability*. 1992. 2, 3, 4
- [20] Quynh Phung, Songwei Ge, and Jia-Bin Huang. Grounded text-to-image synthesis with attention refocusing. In *Proceedings of the IEEE/CVF Conference on Computer Vision and Pattern Recognition*, pages 7932–7942, 2024. 1
- [21] Dustin Podell, Zion English, Kyle Lacey, Andreas Blattmann, Tim Dockhorn, Jonas Müller, Joe Penna, and Robin Rombach. SDXL: Improving latent diffusion models for high-resolution image synthesis. In *The Twelfth International Conference on Learning Representations*. 1
- [22] Robin Rombach, Andreas Blattmann, Dominik Lorenz, Patrick Esser, and Björn Ommer. High-resolution image synthesis with latent diffusion models. In *Proceedings of the IEEE/CVF Conference on Computer Vision and Pattern Recognition*, pages 10684–10695, 2022. 1
- [23] Christoph Schwab and Radu Alexandru Todor. Karhunen–Loève approximation of random fields by generalized fast multipole methods. *Journal of Computational Physics*, 217(1):100–122, 2006. 3
- [24] Jiaming Song, Chenlin Meng, and Stefano Ermon. Denoising Diffusion Implicit Models. In *International Conference on Learning Representations (ICLR)*. arXiv, 2021. 1, 2, 3, 5, 6, 8
- [25] Yang Song, Prafulla Dhariwal, Mark Chen, and Ilya Sutskever. Consistency models. In *Proceedings of the 40th International Conference on Machine Learning*, pages 32211–32252, 2023. 2, 3
- [26] Yang Song and Stefano Ermon. Generative Modeling by Estimating Gradients of the Data Distribution, Oct. 2020. 3
- [27] Yang Song, Liye Shen, Lei Xing, and Stefano Ermon. Solving Inverse Problems in Medical Imaging with Score-Based Generative Models. In *International Conference on Learning Representations (ICLR)*. arXiv, 2022. 1
- [28] Yang Song, Jascha Sohl-Dickstein, Diederik P. Kingma, Abhishek Kumar, Stefano Ermon, and Ben Poole. Score-Based Generative Modeling through Stochastic Differential Equations. In *International Conference on Learning Representations*. arXiv, Feb. 2021. 1, 2, 3, 5, 6
- [29] Danni Yang, Ruohan Dong, Jiayi Ji, Yiwei Ma, Haowei Wang, Xiaoshuai Sun, and Rongrong Ji. Exploring phrase-level grounding with text-to-image diffusion model. In *European Conference on Computer Vision*, pages 161–180. Springer, 2024. 1
- [30] Lvmin Zhang, Anyi Rao, and Maneesh Agrawala. Adding conditional control to text-to-image diffusion models. In *Proceedings of the IEEE/CVF International Conference on Computer Vision*, pages 3836–3847, 2023. 1
- [31] Wendi Zheng, Jiayan Teng, Zhuoyi Yang, Weihang Wang, Jidong Chen, Xiaotao Gu, Yuxiao Dong, Ming Ding, and Jie Tang. Cogview3: Finer and faster text-to-image generation via relay diffusion. In *European Conference on Computer Vision*, pages 1–22. Springer, 2024. 1
- [32] Nicolas Zilberstein, Chris Dick, Rahman Doost-Mohammady, Ashutosh Sabharwal, and Santiago Segarra. Annealed Langevin Dynamics for Massive MIMO Detection. *IEEE Transactions on Wireless Communications*, 22(6):3762–3776, June 2023. 1
- [33] Nicolas Zilberstein, Ashutosh Sabharwal, and Santiago Segarra. Solving Linear Inverse Problems Using Higher-Order Annealed Langevin Diffusion. *IEEE Transactions on Signal Processing*, 72:492–505, 2024. 1

## Appendix

In this appendix, we provide the more ablation study, theory materials and visual results.

### A. Comparisons between KL models with different number of terms in truncated KL expansion

In this section, we show the impacts of hyperparameter  $M$  in KL models on MNIST-32 dataset, which is the number of terms in the truncated expansion. First, we fixed the time discretization as  $N = 20$  and change the  $M$ . As shown in Figure 6(a),  $M = 8$  is the best. Then we consider KL models satisfying that  $NM = 200$ , or in other words, the number of network evaluations (if basis-wise parallelization disabled) in sampling procedure is fixed as 200. As shown in Figure 6(b),  $M = 10$  and  $N = 20$  is the best. The increasing of  $M$  will implicitly increase the model capacity, but also increase the randomness along time, since it finally converges to the vanilla diffusion driven by Brownian motion. The optimal performance achieved near  $M = 10$  by our experiments.

### B. General case or Karhunen Loève Expansion

Generally, for a zeros-mean stochastic process  $X_t$  and an orthogonal set of functions  $\{\phi_m(t)\}$  defined on the interval  $[0, T]$ , the KL expansion of  $X_t(\omega)$  is given by

$$X_t(\omega) = \sum_{m=1}^{\infty} Z_m(\omega) \phi_m(x) \quad (26)$$

$$Z_m(\omega) = \int_0^T X_t(\omega) \phi_m(t) dt. \quad (27)$$

Assuming that these random variables are orthogonal, we have:

$$E(Z_i Z_j) = \lambda_i \delta_{ij}$$

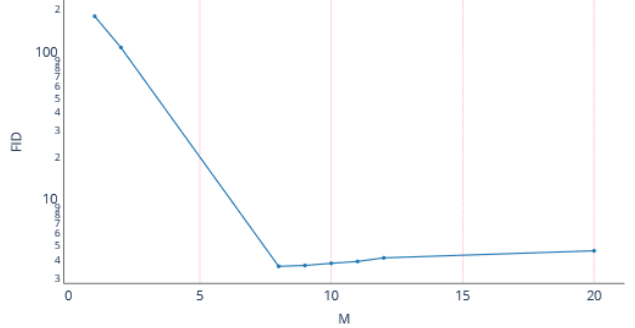
where  $\lambda_n$  are positive numbersto be determined later. Given that an expansion of the form of  $X_t(\omega)$  exists, we can compute the autocovariance function:

$$R(t, x) = E(X_t X_s) = \sum_{m=1}^{\infty} \lambda_m \phi_m(t) \phi_m(s)$$

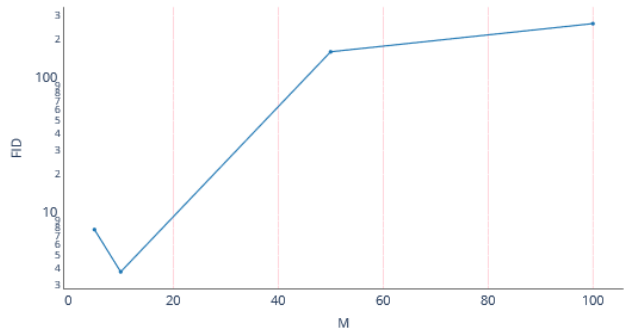
and it follows that

$$\int_0^T R(t, s) \phi_m(s) ds = \lambda_m \phi_m(t)$$

Consequently, for the expansion to be valid, the set  $\{\lambda_m, \phi_m(t)\}$  must consist of the eigenvalues and eigenvectors of the integral operator whose kernel is the correlation function  $R(t, s)$  of  $X_t$ , as described. The above formulas can be solved numerically by performing eigenvalue decomposition of the correlation operator.



(a)



(b)

Figure 6. Illustrate the impacts of hyperparameter  $M$  in the truncated KL expansion. In (a) we fixed time discretization to  $N = 20$ , and in (b) we fix  $MN = 200$ .

### C. More visualization of samples

In this subsection we provide more visualizations of our KL models in Figure 7, 8 and 9, corresponding to the comparisons in Section 6.3.

### D. More comparison experiments for our KL models

In this section, we present additional comparative experiments between the baseline and our KL models. We further train the Baseline-b16 model and our KL-8d-b16 model on the CelebAHQ-128 dataset to evaluate performance on higher-resolution data compared to the CelebAHQ-64 dataset.

Due to time and resource constraints, we conduct 120k optimization steps for the **Baseline-b16** model and 60k steps for our **KL-8d-b16** model. The results shown in Figure 10 indicate that our method achieves a better FID score within 6k steps. A speed-up more that 3-times is achieved. Given the steep decline in the FID score during this initial

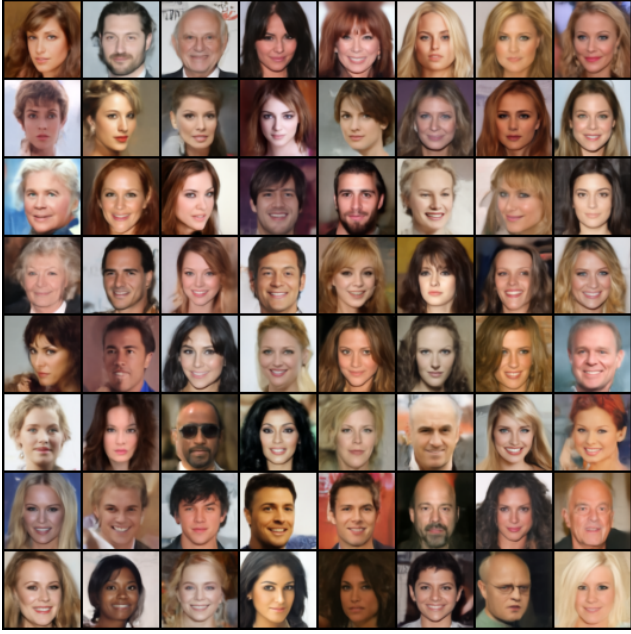


Figure 7. Samples from KL-10d-b16 (FID=13.93) trained with 80k optimizing steps on CelebAHQ-64 dataset.

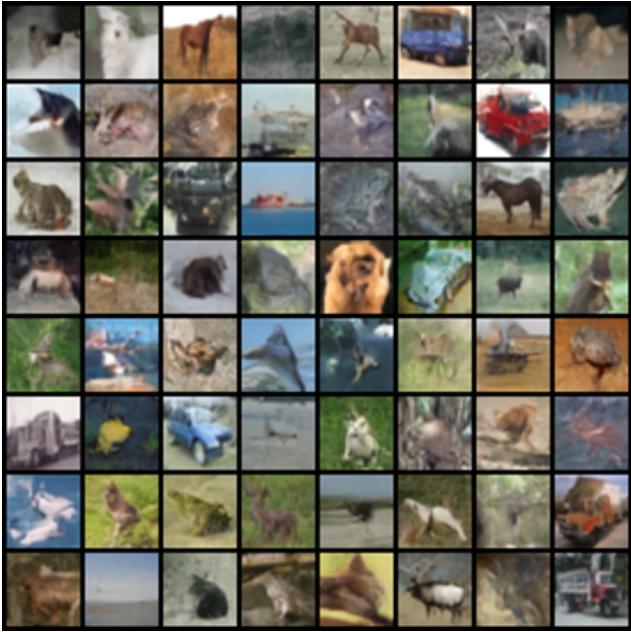


Figure 8. Samples from KL-10d-b64 (FID=25.10) trained with 140k optimizing steps on CIFAR10-32 dataset.

phase, we anticipate that our method would yield even more significant improvements with complete training.



Figure 9. Samples from KL-8d-b32 (FID=3.76) trained with 80k optimizing steps on MNIST-32 dataset.

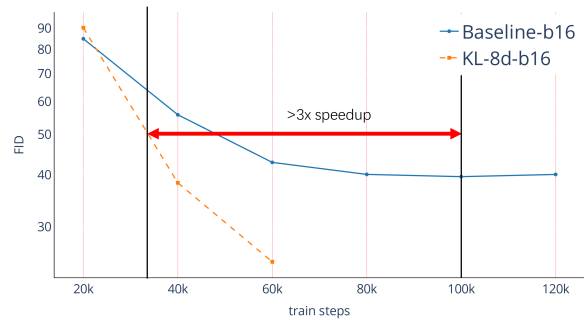


Figure 10. Comparison between the baseline with KL diffusion on CelebAHQ-128 datasets.